OPEN ACCESS
IOP Publishing
Journal of Physics G: Nuclear and Particle Physics
J. Phys. G: Nucl. Part. Phys. **49** (2022) 055102 (25pp)
https://doi.org/10.1088/1361-6471/ac58b3

Towards modeling cluster structure of ^{8}Be with chiral interaction

Tokuro Fukui[1,*]

Yukawa Institute for Theoretical Physics, Kyoto University,
Kitashirakawa Oiwake-Cho, Kyoto 606-8502, Japan

E-mail: tokuro.fukui@yukawa.kyoto-u.ac.jp

Received 10 November 2021, revised 30 January 2022
Accepted for publication 25 February 2022
Published 28 March 2022

Abstract

How the nuclear force behaves in cluster states, in particular those consisting of the α clusters, has been investigated so far, but not yet elucidated. Today the chiral effective field theory (EFT) is established and it would shed new light on the microscopic understanding of the cluster states. We aim to address a possible source of the attraction in the cluster states of ^{8}Be in view of the pion exchange. Namely, we investigate whether the two-pion-exchange interaction acts as a dominant attraction in the $\alpha + \alpha$ system as predicted by a previous work. We describe theoretically the cluster structure of ^{8}Be by the Brink model, for which the effective interaction is designed from the realistic nuclear force derived through the chiral EFT. The two-body matrix elements of the chiral interaction with the local-Gaussian bases are formulated within the approximation of the spin–isospin saturation forming an α particle. Introducing a global prefactor to the chiral interaction phenomenologically, the ground and low-lying excited states of ^{8}Be, the scattering phase shift of the α–α system as well, are satisfactorily depicted. The attraction in the cluster states is found to be stemming from the two-pion-exchange contributions dominantly, along with nonnegligible short-range terms. The present work can be the foundation towards constructing realistic cluster models, by which the cluster states will be revealed microscopically in the next step.

Keywords: cluster states, chiral effective field theory, ^{8}Be

(Some figures may appear in colour only in the online journal)

[1]Present address: RIKEN Nishina Center, Wako 351-0198, Japan
[*]Author to whom any correspondence should be addressed.

1. Introduction

Clustering is one of the fundamental aspects of many-body nuclear systems. With the aim of understanding cluster states of light nuclei in view of realistic nuclear force, an enormous number of theoretical studies have been carried out so far. For instance, there have been approaches to the microscopic description of α-cluster structure and its scattering based on the Brueckner generator coordinate method (GCM) [1–3], the Brueckner antisymmetrized molecular dynamics [4–7], the quantum Monte Carlo methods [8–10], the no-core shell model (NCSM) [11–16], the symmetry-adapted NCSM [17–19], the NCSM with the resonating-group method [20, 21], the NCSM with continuum [22], the fermionic molecular dynamics [23, 24], and the nuclear lattice effective field theory (EFT) [25–33]. We also refer the readers to a recent review paper [34] on related topics.

In spite of intensive studies by the above works, the mechanism how nucleons gain the attraction in the α-cluster states needs to be further clarified. In reference [35] the two-pion (2π)-exchange interaction was assumed to be a source of the attraction in the α-cluster states of ^{8}Be, relying on the fact that there is no attraction stemming from the one-pion (1π) exchange in the direct term (Hartree term) between nucleons, each of which belongs to different α particles. However, this assumption has not been confirmed yet. In the 1960s, when reference [35] was published, the dynamics of nucleons and pions had not been fully revealed. Today, we understand that such dynamics is constrained by the chiral symmetry, and the chiral EFT [36–38] based on this symmetry controls the pion-exchange contributions of the nuclear force in a hierarchical way. Thus, we expect the above assumption can be inspected by employing the chiral interaction.

An important concept to characterize the α clustering is 'internally strong but externally weak' [39, 40], indicating that each of α particles is bound strongly but they weakly interact with each other. The Volkov interaction [41], a phenomenological effective interaction commonly employed, realizes the above nature, namely 'externally weak', by introducing the unnaturally strong odd-state repulsion. In contrast, by a microscopic approach of the Brueckner-GCM [1], the property 'externally weak' was explained by the realistic tensor force, which becomes weaker in ^{8}Be compared to that in ^{4}He. Thus, the saturation mechanism was naturally understood. It is intriguing to investigate the above concept from the view point of the chiral EFT.

In the present work, we concentrate on the typical cluster states of ^{8}Be in the $\alpha + \alpha$ configuration, and aim to address which terms of the chiral interaction (the contact, 1π-exchange, and/or 2π-exchange contributions) account for the origin of the attraction in the α-cluster states, using a simple model. To this end, we adopt the Brink model [42] presuming the spin–isospin saturation forming an α particle. The effective interaction relevant to the Brink model is phenomenologically prepared from the realistic nucleon–nucleon interaction of the chiral EFT at next-to-next-to-next-to-leading order (N^{3}LO), where a high-precision nuclear potentials are available [38, 43–45].

We emphasize that the relative strengths among the contact, 1π-exchange, and 2π-exchange contributions, are expected to be unchanged in the effective interaction in the present work. This is the reason why we employ a phenomenological approach, which is sufficient to fulfill our purpose that we address only the source of the attraction in the $\alpha + \alpha$ system. Of course, what we can elucidate in this paper is limited. Therefore, we regard this work as the first step towards fully microscopic approaches, by which the whole picture of the nuclear force in the clustering is expected to be revealed. Indeed, the two-body matrix elements (MEs) of the chiral

interaction at N^{3}LO within the local-Gaussian states formulated here is applicable to realistic cluster models such like the Brueckner GCM.

This article is organized as follows. Section 2 is devoted to the overview of the theoretical framework, namely the Brink model and the effective Hamiltonian. In section 3, the calculated energies, radii, and phase shifts are compared with the measured data. We also argue the possible source of the attraction in the α-cluster states. A summary and future perspectives are given in section 4. We show in appendix A that our conclusion is robust against the variation of parameters we use. The formalism of the two-body MEs is relegated to appendix B. The constants we adopt are listed in appendix C.

2. Theoretical framework

2.1. Brink model

We describe the cluster states by the Brink model [42], where the single-particle wave function is given by

$$\langle \boldsymbol{r}|\phi_i\chi_a\rangle = \phi_i(\boldsymbol{r})|\chi_a\rangle = \left(\frac{2\nu}{\pi}\right)^{\frac{3}{4}} \exp\left[-\nu(\boldsymbol{r}-\boldsymbol{R}_i)^2\right]|\chi_a\rangle. \tag{1}$$

Here $\boldsymbol{r}$ is the position of nucleon, while $\boldsymbol{R}_i$ is the position of the α clusters, and ν determines the range of the Gaussian. The index a specifies the spin–isospin states;

$$|\chi_a\rangle = \begin{cases} |\uparrow_\sigma\uparrow_\tau\rangle & (a=1), \\ |\uparrow_\sigma\downarrow_\tau\rangle & (a=2), \\ |\downarrow_\sigma\uparrow_\tau\rangle & (a=3), \\ |\downarrow_\sigma\downarrow_\tau\rangle & (a=4), \end{cases} \tag{2}$$

where $\uparrow_\sigma$ and $\downarrow_\sigma$ stand for the spin-up and spin-down states, respectively, and similar to the isospin with the symbol τ. Within the Brink model, the α cluster is presumed as the spin–isospin-saturated four nucleons, i.e. the $(0s)^4$ configuration is adopted. Naturally, the Brink model is tailored for systems described as α clusters only. In such an ansatz, the many-body wave function is given by the Slater determinant as

$$\begin{aligned} |\Psi_{\rm Brink}\rangle = \sqrt{A!}\hat{\mathcal{A}}_A \big[&|\phi_1\chi_1\rangle|\phi_1\chi_2\rangle|\phi_1\chi_3\rangle|\phi_1\chi_4\rangle \\ &\times |\phi_2\chi_1\rangle|\phi_2\chi_2\rangle|\phi_2\chi_3\rangle|\phi_2\chi_4\rangle \\ &\quad\vdots \\ &\times |\phi_{N_\alpha}\chi_1\rangle|\phi_{N_\alpha}\chi_2\rangle|\phi_{N_\alpha}\chi_3\rangle|\phi_{N_\alpha}\chi_4\rangle\big], \end{aligned} \tag{3}$$

with the number of the α particles $N_\alpha = A/4$. Here, four nucleons are located in a point of the coordinate space by sharing the same Gaussian center $\boldsymbol{R}_i$, while their spin and isospin states are different with each other to form an α particle. The A-body antisymmetrizer $\hat{\mathcal{A}}_A$, which is a projection operator, is expressed symbolically as

$$\hat{\mathcal{A}}_A = \frac{1}{A!}\sum_P (-)^P \hat{P}. \tag{4}$$

The summation over P results in $A!$ terms, and $(-)^P$ is 1 or -1 depending on the even or odd permutation respectively. The permutation operator $\hat{P}$ is symbolic of any possible permutation. For example, the two- and three-body antisymmetrizers can be respectively written by

$$\hat{\mathcal{A}}_2 = \frac{1}{2}\left(\mathbb{1} - \hat{\mathcal{P}}_{12}\right), \tag{5}$$

$$\hat{\mathcal{A}}_3 = \frac{1}{3!}\left(\mathbb{1} - \hat{\mathcal{P}}_{12} - \hat{\mathcal{P}}_{23} - \hat{\mathcal{P}}_{31} + \hat{\mathcal{P}}_{12}\hat{\mathcal{P}}_{23} + \hat{\mathcal{P}}_{12}\hat{\mathcal{P}}_{31}\right), \tag{6}$$

where $\hat{\mathcal{P}}_{12}$ is the permutation operator exchanging the particles 1 and 2.

The many-body states $|\Psi_{\rm Brink}\rangle$ are projected onto the eigenstates of the angular momentum J as

$$|\Psi^J_{MM'}\rangle = \frac{2J+1}{8\pi^2}\int {\rm d}\Omega\, D^{J*}_{MM'}(\Omega)\hat{R}(\Omega)|\Psi_{\rm Brink}\rangle, \tag{7}$$

where $D^J_{MM'}$ is the Wigner D-function with the eigenvalues M and M' of the z-component of J, while $\hat{R}$ is the rotation operator acting on the coordinate and spin states. The integration over the three-dimensional Euler angle Ω is performed numerically.

As regards ^{8}Be, two α clusters can be settled in a one-dimensional configuration, namely $\boldsymbol{R}_1 = d\boldsymbol{e}_z/2$ and $\boldsymbol{R}_2 = -d\boldsymbol{e}_z/2$ with the unit vector $\boldsymbol{e}_z$ of the three-dimensional Cartesian coordinates. When the Hamiltonian is given, the corresponding energy eigenvalues can be obtained as a function of the α–α relative distance d within the limit of the single-Slater determinant.

In order to describe the system more precisely, we superpose the Slater determinants associated with different values of d based on the GCM [42, 46, 47] as

$$|\Psi^J_{MM'}\rangle_{\rm GCM} = \sum_k c_k |\Psi^J_{MM'}(d_k)\rangle. \tag{8}$$

Here the subscript k of d is shown explicitly. The coefficient c_k is obtained by solving the Hill–Wheeler equation [42, 46, 47]. The phase shift of the α–α scattering is also calculated based on the Kohn–Hulthén variational principle with the GCM [48, 49].

Since the α-cluster structure is presumed, we cannot discuss the intrinsic structure of ^{4}He by the Brink model. Therefore, the calculated energy of ^{4}He is always subtracted from that of ^{8}Be, as explained in section 3.1, and thus we address the relative energy of the ^{8}Be-ground state measured from the $\alpha + \alpha$ threshold.

2.2. Hamiltonian

The many-body Hamiltonian in the present framework is given by

$$\hat{H} = \sum_{i=1}^{A}\hat{T}_i - \hat{T}_G + \sum_{i<j}^{A}\left[\hat{V}^{\rm (N)}_{ij} + \hat{V}^{\rm (C)}_{ij}\right], \tag{9}$$

where $\hat{T}_i$ is the kinetic-energy operator of the ith nucleon and that of the center-of-mass contribution $\hat{T}_G$ is subtracted. We here consider only the two-body interaction consisting of the nuclear interaction $\hat{V}^{\rm (N)}_{ij}$ and the Coulomb interaction $\hat{V}^{\rm (C)}_{ij}$.

We employ the chiral interaction at N^{3}LO [38, 43–45] as $\hat{V}^{\rm (N)}_{ij}$, which can be classified into seven terms as

$$\hat{V}^{\rm (N)}_{ij} = \hat{V}^{(0)}_{\rm ct} + \hat{V}^{(0)}_{1\pi} + \hat{V}^{(2)}_{\rm ct} + \hat{V}^{(2)}_{2\pi} + \hat{V}^{(3)}_{2\pi} + \hat{V}^{(4)}_{\rm ct} + \hat{V}^{(4)}_{2\pi}. \tag{10}$$

Using the chiral-expansion power n_χ, the superscripts stand for the interaction at leading order (LO) with $n_\chi = 0$, next-leading order (NLO) with $n_\chi = 2$, next-to-next-to-leading order (N^2LO) with $n_\chi = 3$, and N^3LO with $n_\chi = 4$. The 2π-exchange interaction $\hat{V}_{2\pi}^{(n_\chi)}$ and the contact interaction $\hat{V}_{\rm ct}^{(n_\chi)}$ depend on n_χ, while the 1π-exchange interaction $\hat{V}_{1\pi}$ contributes only at LO.

Then we need to derive the effective Hamiltonian $\hat{H}_{\rm eff}$ relevant to the Brink model from the realistic Hamiltonian $\hat{H}$. In order to be consistent with the concept of constructing realistic nuclear forces, a microscopic way to derive $\hat{H}_{\rm eff}$ such as the Brueckner-GCM approach is necessary. However, in this paper, we obtain $\hat{H}_{\rm eff}$ in a phenomenological way as the first step towards the realistic cluster model based on the Brueckner theory. We introduce the prefactor c_0, and thus $\hat{H}_{\rm eff}$ is given by

$$\hat{H}_{\rm eff} = \sum_{i=1}^{A} \hat{T}_i - \hat{T}_G + \sum_{i<j}^{A} \left[\hat{V}_{ij}^{(\rm N;eff)} + \hat{V}_{ij}^{(\rm C)} \right], \tag{11}$$

$$\hat{V}_{ij}^{(\rm N;eff)} = c_0 \hat{V}_{ij}^{(\rm N)}. \tag{12}$$

The prefactor c_0 is fixed so that the relative energy of the ^{8}Be-ground state measured from the $\alpha + \alpha$ threshold obtained with the GCM coincides with the experimental value.

Here we emphasize that, in spite of the introduction of the phenomenological prefactor globally, the relative strength of each term of the chiral interaction remains realistic, i.e. the low-energy constants (LECs) are unchanged from those of the realistic force. Therefore we can address which term of the interaction in view of the pion exchange plays an essential role on the cluster states. In appendix A.1 we show that our conclusion is robust against the variation of c_0 from unity to a certain value fixed by the strategy mentioned above.

In the Brink model, due to the ansatz of the spin–isospin saturation with respect to the α particle, the antisymmetrized two-body MEs of the noncentral terms involved in $\hat{V}_{ij}^{(\rm N)}$ become zero. In appendix B we formulate the two-body MEs of the chiral interaction at N^3LO within the Brink model. The formalism of the two-body MEs is applicable to the Brueckner–Brink/GCM model, which will be constructed in future.

As mentioned in section 1, the effective interaction derived from the Brueckner theory, which can handle the tensor force in a straight-forward way, is desirable to account for the concept 'internally strong but externally weak'. In the present approach, however, the introduction of c_0 may not be adequate to explain this concept, namely 'internal strong'. Instead, this paper provides a basis towards such a fully microscopic approach. Therefore, the derivation of the effective interaction by the Brueckner theory starting from the chiral-EFT interaction will be a vital work in future, and thus, the tensor-force effect and three-nucleon force of the chiral interaction on the clustering will be clarified.

Furthermore, we comment on the noncentral contribution to the cluster states of ^{8}Be, in particular the tensor-force effect. In references [50, 51], within the framework of the antisymmetrized quasicluster model, the authors have shown that the tensor force plays a dominant role inside ^{4}He, corresponding to the shift of the 2α's-threshold energy. It results in the tensor-force effect acting repulsively in the relative energy of the ^{8}Be-ground state measured from the threshold, when the two clusters approach.

2.3. Model setup

The size parameter ν is fixed so that the calculated root-mean-square (RMS) matter radius $R_{\rm M}$ of ^{4}He is consistent with the observed value $R_{\rm M}^{(\rm exp)} = 1.45$ fm. Note that $R_{\rm M}^{(\rm exp)}$ is extracted from

Table 1. The prefactor c_0 fixed by the comparison of the GCM-calculated relative energy of the ^{8}Be-ground state with measured values.

	$\Lambda = 450$ MeV	$\Lambda = 500$ MeV	$\Lambda = 600$ MeV
c_0	1.37	1.79	2.15

$R_{\rm M}^{(\rm exp)} = \sqrt{R_{\rm C}^2 - R_{\rm p}^2 - (N/Z)R_{\rm n}^2}$ with the proton and neutron numbers Z and N, respectively, the measured charge radius $R_{\rm C} = 1.68$ fm [52] of ^{4}He, and the squared proton (neutron) charge radius, experimentally obtained as $R_{\rm p}^2 = 0.832$ fm^2 [53] ($R_{\rm n}^2 = -0.115$ fm^2 [52]). Choosing $\nu = 0.26$ fm^{-2}, corresponding to the harmonic-oscillator energy, $\hbar\omega = 2\hbar^2\nu/m_{\rm N} \sim 22$ MeV, we compute $R_{\rm M}$ as 1.47 fm, where $m_{\rm N}$ is the average nucleon mass. Although the choice of $\nu = 0.26$ fm^{-2} gives the proper $R_{\rm M}$, our model cannot result in the reasonable value of the ^{4}He-ground-state energy at the same time, as shown in section 3. Therefore, in appendix A.2, we investigate the sensitivity to ν in the description of the ^{8}Be-cluster state, and confirm the validity of the current value of ν.

We test three sets of the parameterization of the chiral interaction, depending on the cutoff Λ, namely, the widely adopted value, $\Lambda = 500$ MeV [38, 45], as well as $\Lambda = 450$ [54, 55] and 600 MeV [38]. The physical constants and LECs we use are summarized in appendix C. The prefactor c_0, which is determined from the comparison of the calculated relative energy of the ^{8}Be-ground state based on the GCM with the measured value, also depends on Λ. Thus, all the calculations below are carried out with $c_0 = 1.37, 1.79$, and 2.15 for $\Lambda = 450, 500$, and 600 MeV, respectively, as listed in table 1. See also appendix A.1, where we show how the results vary when c_0 is evolved from unity to the value given in table 1.

The GCM calculations are performed with the twelve Slater determinants (the maximum value of k is 12) specified by d_k from 1.0 to 8.7 fm with the 0.7 fm interval. The same basis functions are applied to the phase-shift calculations.

3. Results and discussion

3.1. Energies, radii, and phase shifts

In table 2, we list the ground-state energy of ^{4}He, denoted by E_α, computed with the present setup. The calculated values of E_α are not far from the experimental data [56], except for the case of $\Lambda = 600$ MeV. Note that, $\hat{H}_{\rm eff}$ with c_0 fixed for the ground state of ^{8}Be does not give the optimal E_α at around $\nu = 0.26$ fm^{-2}. Therefore, the description of ^{4}He must be improved in a forthcoming work, where $\hat{H}_{\rm eff}$ will be derived in a fully microscopic way.

In order to address the relative motion of the clusters, we define the relative energy $E(J^\pi)$ of ^{8}Be measured from the $\alpha + \alpha$ threshold as

$$E(J^\pi) = E_{\rm Be}(J^\pi) - 2E_\alpha, \tag{13}$$

where $E_{\rm Be}(J^\pi)$ is the eigenenergy of $\hat{H}_{\rm eff}$ associated with the total spin and parity J^π state of ^{8}Be, and E_α listed in table 2 are used.

Figure 1 shows the calculated results of $E(0^+)$ as a function of the α–α distance d. The solid, dashed, and dotted lines are obtained with $\Lambda = 450, 500$, and 600 MeV, respectively. One finds that the energy minimum appears at $d \sim 3.0$ fm with the 450 MeV cutoff and $d \sim 3.5$ fm with the other cutoff values. Since the 450 MeV-cutoff potential is less repulsive compared to that of the higher cutoffs, it describes the more compact ground state of ^{8}Be. In reference

Table 2. The ground-state energy of ^{4}He calculated with $\hat{H}_{\rm eff}$ defined by equation (11). The experimental value given in the rightmost column is taken from reference [56].

	$\Lambda = 450$ MeV	$\Lambda = 500$ MeV	$\Lambda = 600$ MeV	Exp
E_α (MeV)	−33.0397	−34.3761	−58.6637	−28.2957

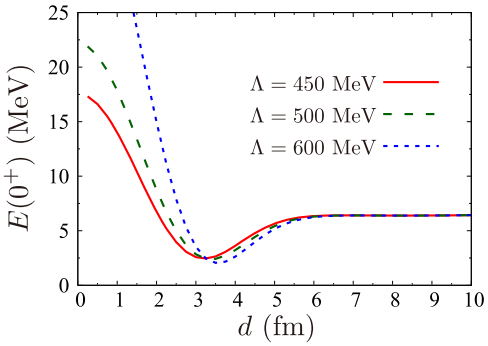

Figure 1. The relative energy $E(0^+)$ of ^{8}Be measured from the $\alpha + \alpha$ threshold as a function of the relative distance between the clusters. The solid, dashed, and dotted lines are the results obtained with the cutoffs $\Lambda = 450$, 500, and 600 MeV, respectively.

[58], it has demonstrated that, if the nucleon–nucleon potential is too repulsive, such energy minimum is not realized. Thus, we find the current parameterization of $\hat{H}_{\rm eff}$ properly accounts for the attraction, and the present results are qualitatively comparable to the results in reference [58], where the phenomenological Volkov-No. 2 [41] and Tohsaki-F1 [59] interactions are employed. The energy curves converge to a constant value at large d. This is because $E(0^+)$ at large d, where the nucleon–nucleon interaction between the clusters vanishes, can be estimated by the center-of-mass kinetic energy, $\hbar\omega/4 \sim 5$ MeV, in addition to the small Coulomb energy.

In figure 2, we compare the low-lying energy spectra of ^{8}Be computed by the GCM with the experimental values [57] displayed in the left side of the figure. Tuning c_0, we obtain the 0^+ energies (0.135, 0.146, and 0.050 MeV, respectively for $\Lambda = 450$, 500, and 600 MeV) that coincide well with the measured energy, and the 2^+ energies are also consistent with the experimental one. The calculations for the 4^+ state overestimate the measured data by a few MeV and become worse for the higher cutoffs. This is probably due to the failure of the bound-state approximation of the present model, which cannot describe properly the 4^+ state as the broad resonance. Indeed, as mentioned below, the scattering phase shift of the $\ell = 4$ state are reasonably depicted, in particular, with $\Lambda = 450$ MeV (see figure 3). We obtain the RMS-matter radius $R_{\rm M}$ of ^{8}Be(0^+) calculated by the GCM as 2.71, 2.76, and 2.79 fm associated with $\Lambda = 450$, 500, and 600 MeV, respectively.

Figure 3 shows the scattering phase shift δ_ℓ with the orbital-angular momentum ℓ associated with the relative motion of the $\alpha + \alpha$ system, as a function of the center-of-mass energy $E_{\rm CM}$ between the clusters up to 50 MeV. The solid, dashed, and dotted curves are the theoretical results corresponding to $\Lambda = 450$, 500, and 600 MeV, respectively. The experimental δ_ℓ represented by the circles are taken from reference [67], in which the original data were compiled from references [60–66]. In figure 3(a), one finds that the three curves slightly underestimate the data of δ_0, whereas the underestimation by the 500 MeV and 600 MeV cutoffs is much more visible for the $\ell = 2$ and 4 cases exhibited in figures 3(b) and (c), respectively, indicating

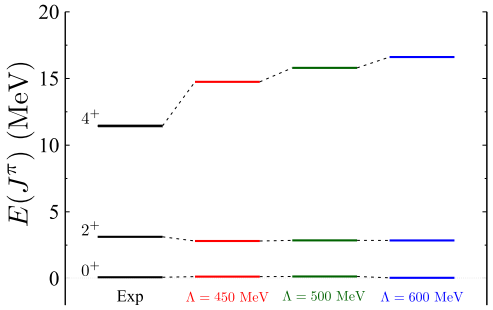

Figure 2. The low-lying spectra of ^{8}Be, referred to the $\alpha + \alpha$ threshold. The calculated levels denoted by $\Lambda = 450, 500$, and 600 MeV are compared with the observed data (Exp) [57] in the left side.

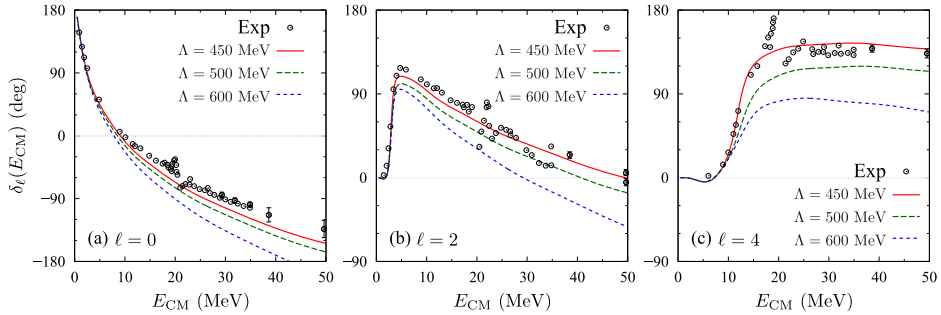

Figure 3. The scattering phase shift of the $\alpha + \alpha$ system of (a) $\ell = 0$, (b) $\ell = 2$, and (c) $\ell = 4$, as a function of the center-of-mass energy. The solid, dashed, and dotted lines, respectively corresponding to the calculated results with the cutoffs $\Lambda = 450, 500$, and 600 MeV, are confronted with the measured data [60–66] represented by the circles.

the lack of the attraction. The 500 MeV- and 600 MeV-cutoff potentials have more contributions from high momentum components compared to the 450 MeV-cutoff case. In addition, these higher-cutoff potentials have relatively small components of the momentum less than the cutoff because of the moderate regulator with small n (see table C2). These characteristics may lead to better results for $\Lambda = 450$ MeV.

Our results on the phase shift are basically consistent with those in reference [67], where the data were reasonably explained by employing a nucleon–nucleon potential of Hasegawa and Nagata [68]. This potential was designed to account for the binding energy of ^{4}He and the α–α scattering phase shift by tuning the even-state attraction of the Tamagaki-A realistic potential [69].

Let us focus on the ground state of ^{8}Be. Even though the 0^+ energies computed with the three values of Λ are almost equivalent with each other as shown in figure 2, the phase shift δ_0 is significantly sensitive to the detail of the Hamiltonian. Indeed, the Λ dependence of the scattering states can be clearly seen in the reduced-width amplitude (RWA), y_ℓ, expressing the α–α relative wave function. The detail of calculating y_ℓ can be found in references [70, 71], and its explicit form is also given in appendix of reference [72]. Figure 4 displays the RWA of $\ell = 0$ multiplied by the relative-cluster coordinate R, as a function of R. The solid, dashed, and dotted lines correspond to the results with $\Lambda = 450, 500$, and 600 MeV, respectively. One finds

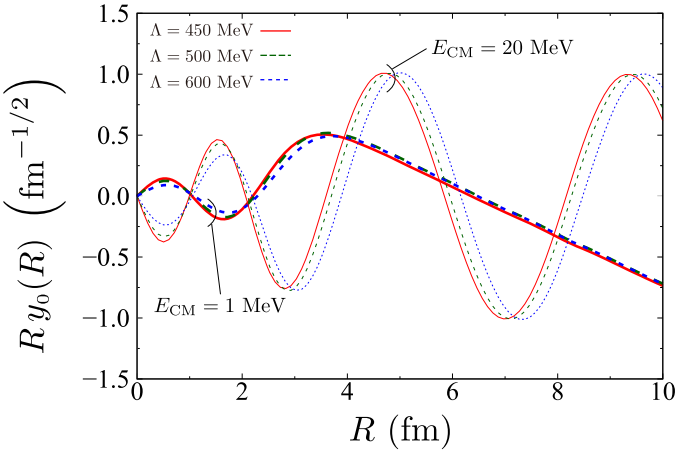

Figure 4. The RWA of the scattering state with the orbital-angular momentum $\ell = 0$ as a function of the relative-cluster distance. The solid, dashed, and dotted lines are obtained using $\Lambda = 450$, 500, and 600 MeV, respectively. The thick lines (thin lines) correspond to $E_{\rm CM} = 1$ MeV (20 MeV).

that, at $E_{\rm CM} = 1$ MeV, where the phase shifts associated with the different Λ are consistent with each other, the RWAs expressed by the thick lines do not strongly depend on Λ. In contrast, at $E_{\rm CM} = 20$ MeV, the deviation of the phase of y_0 is visible among the thin lines, in accordance with the difference appearing in the phase shift. The similar correspondence between the phase shift and RWA is confirmed for the $\ell = 2$ and 4 states, although the Λ dependence of the RWA becomes drastic in these excited states.

3.2. Possible origin of attraction

Since the direct 1π exchange between nucleons inside the different α particles is forbidden, sources of the attraction in the α-cluster states need to be verified. In order to make the discussion clear, we put our focus on the ground state of ^{8}Be. We show $E(0^+)$ as a function of d in figure 5, where the solid, dashed, dotted, and dash–dotted lines are obtained with the full contributions $\hat{V}^{(\rm N)}_{ij}$ defined by equation (10), the contacts $\hat{V}^{(0)}_{\rm ct} + \hat{V}^{(2)}_{\rm ct} + \hat{V}^{(4)}_{\rm ct}$, the 1π-exchange term $\hat{V}^{(0)}_{1\pi}$, and the 2π-exchange terms $\hat{V}^{(2)}_{2\pi} + \hat{V}^{(3)}_{2\pi} + \hat{V}^{(4)}_{2\pi}$, respectively. The corresponding values of E_α are listed in table 3. We employ c_0 given in table 1. As expected, the 1π-exchange interaction in the $\alpha + \alpha$ system is crucially repulsive, expressed by the dotted lines. The contact interactions corresponding to the dashed lines are repulsive at small d, but they seem to act attractively for $\Lambda = 500$ and 600 MeV (450 MeV) at $d \sim 4.0$ fm ($\sim$3.5 fm), where the energy minimum is produced, being qualitatively consistent with the results of the full calculations. How the separated nucleons interact with each other via the contact force is explained later. The 2π-exchange interactions are strongly attractive, and thus we confirm the assumption [35] that the main source of the attraction stems from these interactions.

Here, we mention two points; (i) the attraction by the 2π-exchange interactions alone is not sufficient to explain the ground-state property of ^{8}Be, and (ii) the 2π-exchange interactions of $\Lambda = 450$ MeV behave quite differently from the others. As regards the point (i), the short-range attraction originating from $\hat{V}^{(0)}_{\rm ct}$ plays also an essential role, consistent with the fact that the energy minimum is realized by the contact interactions alone in figure 5. The attraction by the LO-contact term is demonstrated in figure 6, where the thick-dashed, thin-solid, thin-dashed,

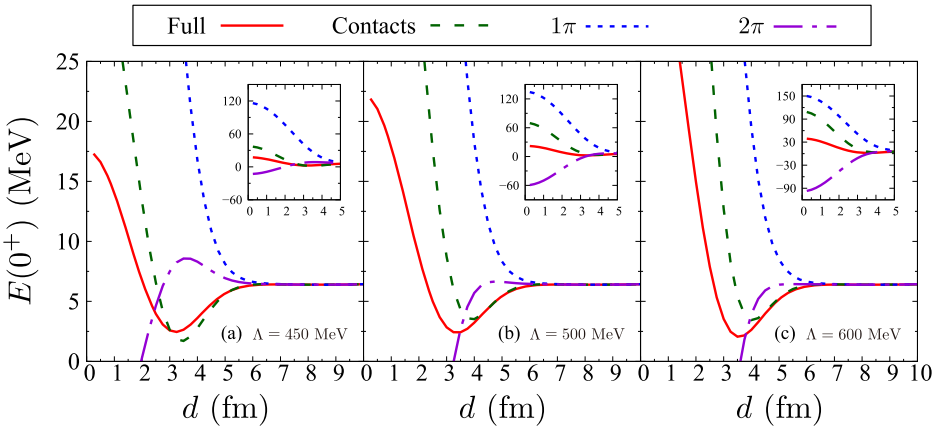

Figure 5. The relative energy of the ^{8}Be-ground state measured from the $\alpha + \alpha$ threshold computed with the chiral interaction at N^{3}LO (solid lines), the contact terms (dashed line), the 1π-exchange term (dotted lines), and the 2π-exchange terms (dash–dotted lines). The results of the cutoffs $\Lambda = 450, 500$, and 600 MeV are shown in the left, middle, and right panels, respectively.

Table 3. Contributions of each pion-exchange term to the ground-state energy of ^{4}He. The value of c_0 fixed from the full contribution is commonly used.

		$\Lambda = 450$ MeV	$\Lambda = 500$ MeV	$\Lambda = 600$ MeV
E_α (MeV)	Full	−33.0397	−34.3761	−58.6637
	Contacts	−22.5984	−16.5547	−33.4038
	1π	97.5687	112.8210	125.9402
	2π	−9.3107	−31.9431	−52.5009

and thin-dotted lines are $E(0^+)$ computed with $\hat{V}^{(0)}_{\rm ct} + \hat{V}^{(2)}_{\rm ct} + \hat{V}^{(4)}_{\rm ct}$ (equivalent to the dashed line in figure 5), $\hat{V}^{(0)}_{\rm ct}$, $\hat{V}^{(2)}_{\rm ct}$, and $\hat{V}^{(4)}_{\rm ct}$, respectively. The values of E_α computed with these terms are given in table 4. In figure 6, one finds that the behavior of energies are qualitatively independent of Λ.

The point (ii) is due to the different constituents of the 2π-exchange terms, namely the N^{2}LO terms $\hat{V}^{(3)}_{2\pi}$ and the N^{3}LO terms $\hat{V}^{(4)}_{2\pi}$, since the LECs c_i of $\Lambda = 450$ MeV are different from those of higher Λ (see table C2). To see this clearly, we show in figure 7 a breakdown of the 2π contributions to $E(0^+)$, computed with $\hat{V}^{(2)}_{2\pi} + \hat{V}^{(3)}_{2\pi} + \hat{V}^{(4)}_{2\pi}$, $\hat{V}^{(2)}_{2\pi}$, $\hat{V}^{(3)}_{2\pi}$, and $\hat{V}^{(4)}_{2\pi}$, respectively represented by the thick-dash–dotted, thin-solid, thin-dashed, and thin-dotted lines. The corresponding calculations for ^{4}He result in E_α given in table 4. One finds that, independently of Λ, $\hat{V}^{(3)}_{2\pi}$ is attractive accounting for the intermediate-range attraction of the nuclear force as we know [38], while $\hat{V}^{(4)}_{2\pi}$ acts repulsively as comparable as $\hat{V}^{(0)}_{1\pi}$. With decreasing Λ, the repulsion by $\hat{V}^{(4)}_{2\pi}$ becomes modest, but the attraction by $\hat{V}^{(3)}_{2\pi}$ is also suppressed, resulting in the less-attractive interaction totally of the 2π-exchange contributions $\hat{V}^{(2)}_{2\pi} + \hat{V}^{(3)}_{2\pi} + \hat{V}^{(4)}_{2\pi}$. The contact terms at LO, $\hat{V}^{(0)}_{\rm ct}$, is another source of the attraction as shown in figure 6, but it is not enough to compensate a loss of attraction in $\hat{V}^{(3)}_{2\pi}$ of $\Lambda = 450$ MeV. The full results are obtained by summing up all individual contributions coherently, and thus, the interference through such a coherent process brings about the whole interaction $\hat{V}^{(\rm N)}_{ij}$ showing relatively

Table 4. A breakdown of the contact and 2π terms contributing to E_α.

		$\Lambda = 450$ MeV	$\Lambda = 500$ MeV	$\Lambda = 600$ MeV
E_α (MeV)	Contact at LO $\hat{V}^{(0)}_{\rm ct}$	−124.4714	−155.1972	−200.8181
	Contact at NLO $\hat{V}^{(2)}_{\rm ct}$	144.9496	187.2175	212.5949
	Contact at N^{3}LO $\hat{V}^{(4)}_{\rm ct}$	55.6226	50.1244	53.5186
	2π at NLO $\hat{V}^{(2)}_{2\pi}$	59.8968	62.7673	66.0032
	2π at N^{2}LO $\hat{V}^{(3)}_{2\pi}$	−78.6510	−127.9064	−173.1798
	2π at N^{3}LO $\hat{V}^{(4)}_{2\pi}$	108.1427	131.8953	153.3750

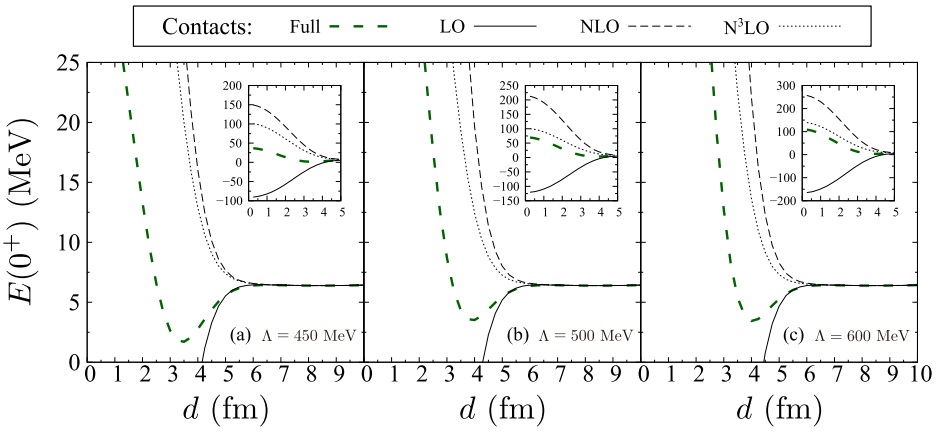

Figure 6. The contact-term contributions to $E(0^+)$. The thick-dashed, thin-solid, thin-dashed, and thin-dotted lines correspond to the results obtained with $\hat{V}^{(0)}_{\rm ct} + \hat{V}^{(2)}_{\rm ct} + \hat{V}^{(4)}_{\rm ct}$, $\hat{V}^{(0)}_{\rm ct}$, $\hat{V}^{(2)}_{\rm ct}$, and $\hat{V}^{(4)}_{\rm ct}$, respectively, for the case of (a) $\Lambda = 450$ MeV, (b) $\Lambda = 500$ MeV, and (c) $\Lambda = 600$ MeV.

weak Λ dependence. Since $E(0^+)$ computed with the contact interactions has the minimum point reasonably, we also investigate the behavior of the phase shift calculated with the contacts alone. Figures 8(a)–(c) show δ_0 computed with $\Lambda = 450, 500$, and 600 MeV, respectively. The thick lines are obtained by the full calculations including up to the N^{3}LO contributions, while the dashed lines correspond to the results of the contact terms. In figure 8(a), the two lines qualitatively agree with each other, although the contact contributions are less attractive, as deduced also from figure 5(a). The gross behavior of the dashed curves in figures 8(b) and (c) is not far from that of the solid line, but we can find a distinguished difference at low $E_{\rm CM}$; an unphysical peak appears around $E_{\rm CM} \sim 1.5$ MeV. This is due to the poor reproduction of $E(0^+)$, which essentially determines the phase shift at lower-scattering energies. Indeed, with the contact terms alone, the GCM calculations result in $E(0^+) = -0.0344, 1.1130$, and 1.1029 MeV for $\Lambda = 450, 500$, and 600 MeV, respectively.

In conclusion, we can state that the attraction between nucleons in the α-cluster states seems to originate dominantly from the 2π-exchange terms, and the contact forces also plays an important role; $\hat{V}^{(3)}_{2\pi}$ and $\hat{V}^{(0)}_{\rm ct}$ are attractive but the other terms are repulsive. An intuitive picture to explain how the contact interactions contribute to a pair of separated nucleons in the cluster states of ^{8}Be is shown in figure 9. The two clusters are located having the relative distance ∼3.0–3.5 fm, as illustrated by the red circles. The Brink model we adopt describes the nucleon

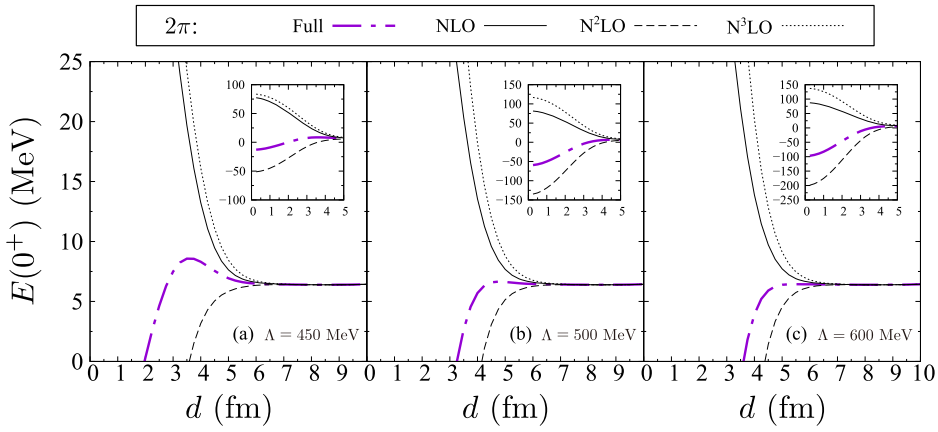

Figure 7. Same as figure 6, but for the 2π contributions, and now the thick-dash–dotted, thin-solid, thin-dashed, and thin-dotted lines are obtained by adopting $\hat{V}^{(2)}_{2\pi} + \hat{V}^{(3)}_{2\pi} + \hat{V}^{(4)}_{2\pi}$, $\hat{V}^{(2)}_{2\pi}$, $\hat{V}^{(3)}_{2\pi}$, and $\hat{V}^{(4)}_{2\pi}$, respectively.

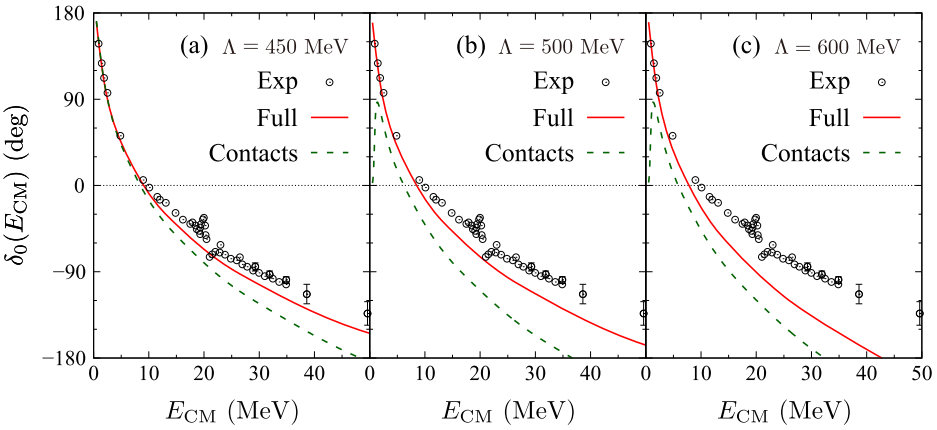

Figure 8. The phase shift of $\alpha + \alpha$ scattering with $\ell = 0$ computed with the chiral interaction at N^{3}LO (solid lines) and the contact terms alone (dotted lines) for (a) $\Lambda = 450$ MeV, (b) $\Lambda = 500$ MeV, and (c) $\Lambda = 600$ MeV.

distribution by the Gaussian-wave packets, the range of which is about 2 fm, corresponding to $\nu = 0.26$ fm^{-2}. The two wave packets, ϕ_1 and ϕ_2, which are settled at the center of each cluster, overlap as expressed by the shadow. Thus, we find that, even if the two clusters are separated from each other, nucleons can interact through the contact forces in the overlap region, besides the main contribution of the attraction by the 2π-exchange interactions. In Ref. [35], where the 2π-exchange interaction was assumed to be a source of the attraction, the authors did not consider the short-range attraction. Instead, they used the short-ranged-repulsive interaction expressed by a Gaussian function of the range $\sim$0.4 fm. Although their assumption is consistent with our outcome, such modeling of the nuclear force seems to result in a picture different from that of the chiral EFT. In reference [32], the chiral interactions at only LO are

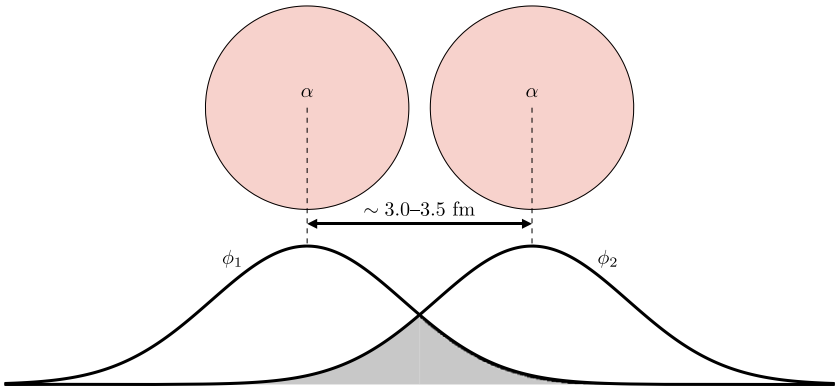

Figure 9. Intuitive picture explaining the mechanism how separated nucleons interact with each other via the contact force. Two α particles are illustrated as the red circles, and the nucleon-wave packets, ϕ_1 and ϕ_2, have the overlap region expressed by the shadow. See the text for detail.

included in the nuclear-lattice EFT, by which the simulations of the eight-nucleon system reasonably explained the α–α phase shift in the low-energy region. The contact-origin attraction they adopted is not in contradiction with our consequence.

At the end of this section, we mention the relationship between the chiral EFT and the conventional meson theory of nuclear forces [73, 74], since it can support our results. Both theories provide high-precision nuclear potentials, which are quantitatively equivalent, and hence, there is the correspondence between them. The 1π-exchange contribution is common but the other contributions are not bijection between both theories. Roughly speaking, the σ-exchange contribution in the meson theory responsible for the intermediate-range attraction is fragmented into the 2π-exchange terms order by order in the chiral EFT, indicating that 2π-exchange contributions $\hat{V}^{(2)}_{2\pi} + \hat{V}^{(3)}_{2\pi} + \hat{V}^{(4)}_{2\pi}$ totally would be attractive. Similarly, the ω-exchange contribution characterizing the repulsive core at short distances corresponds naively to the chiral-contact terms order by order [38], and thus we expect $\hat{V}^{(0)}_{\rm ct} + V^{(2)}_{\rm ct} + \hat{V}^{(4)}_{\rm ct}$ would be repulsive at short distances. These correspondences are consistent with our results, although, as mentioned above, they are not bijection completely. Hence, one of the 2π-exchange (contact) contributions can be repulsive (attractive), as confirmed by our calculations.

4. Summary and perspectives

With the aim of searching the possible source of the attraction in the cluster states of ^{8}Be, we have phenomenologically prepared the effective interaction originating from the chiral EFT, which can classify the pion-exchange contributions order by order. Although we have introduced the phenomenological prefactor into the chiral potential, the LECs are unchanged, and thus the relative contributions of each term of the chiral interaction remain realistic.

Adopting the Brink model, the relative energy of ^{8}Be measured from the two-α threshold has been calculated and it has found to have a minimum point around 3.0 to 3.5 fm of the α–α relative distance. Performing the GCM calculations with respect to the relative-cluster distance as the generator coordinate, we have computed the low-lying energy spectra and the scattering phase shift, which are satisfactorily comparable to the experimental data.

We have investigated the individual contributions of the pion-exchange interactions at each chiral-expansion order, and found that the 2π-exchange terms can be a dominant source of the attraction in the ground state of ^{8}Be, confirming the assumption of the previous work [35]. However, the short-range attraction originating from the contact terms in addition to the 2π-exchange interactions is also the important mechanism relevant to the α-cluster states.

Our outcome in the present paper is not based on a fully microscopic approach, and therefore further investigation is necessary, since (I) we have introduced a phenomenological prefactor, and (II) the three-nucleon force and the tensor-force effect are disregarded. To overcome the point (I), we are now working on constructing cluster models based on the Brueckner theory to microscopically drive the effective Hamiltonian starting from the chiral interaction. It will be interesting to investigate whether the individual contributions of the chiral interaction remain unchanged in the effective interaction after solving the Bethe–Goldstone equation with the original force. The formalism of the two-body MEs reported in the present article is applicable to such models. In parallel with the construction of the realistic cluster model with the chiral interaction, in order to tackle the point (II), we will take into account the chiral three-nucleon force at N^{2}LO [37, 38, 75, 76], which is dominated by the 2π-exchange terms, contributing to the tensor force. As demonstrated in reference [77] the chiral three-nucleon force acts attractively in the *p*-shell nuclei including ^{8}Be, while the two-body tensor force provides repulsive effect [50, 51]. The interplay between them in the cluster states of ^{8}Be needs to be clarified to draw a robust conclusion on the origin of the attraction on such states.

Acknowledgments

The author thanks N Itagaki for helpful advice and providing a numerical code of the Brink model. He also thanks M Kamimura for supplying a numerical code to calculate the scattering phase shift, and R Machleidt for parameterizing the LECs. He is grateful to Y Yamaguchi for fruitful discussions. This work was supported in part by JSPS KAKENHI Grant No. JP21K13919. The calculations have been carried out using the computer facilities at Yukawa Institute for Theoretical Physics, Kyoto University, and Research Center for Nuclear Physics, Osaka University.

Data availability statement

The data that support the findings of this study are available upon reasonable request from the authors.

Appendix A. Investigation of parameter dependence

A.1. Global prefactor

Here, we discuss how the results depend on the variation of c_0 from unity to the value fixed from the relative energy of the ^{8}Be-ground state, listed in table 1. Figure A1 displays $E(0^+)$ as a function of d computed with each term of the interaction of $\Lambda = 450$ MeV. In figures A1(a)–(d), where the legends are same as those in figure 5, c_0 is varied gradually from 1.00 to 1.37. Independently of c_0, we can draw the conclusion as in section 3.2, i.e. the 2π-exchange interaction plays a dominant role for the attraction for the cluster state, the 1π-exchange interaction is strongly repulsive, and the contact interaction acts attractively at $d \sim 3.5$ but basically repulsive at the short distances. Note that the corresponding energies of ^{4}He is listed in table A1. Figures A1(e)–(h) represent the c_0 dependence of $E(0^+)$ for the full contribution, contact

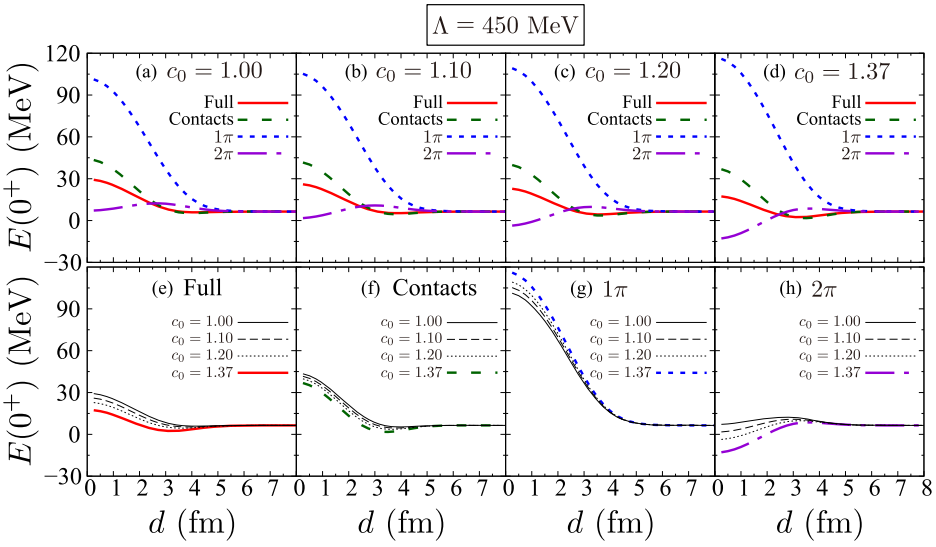

Figure A1. The c_0 dependence of $E(0^+)$ of ^{8}Be for the $\Lambda = 450$ MeV case. (a)–(d) The solid, dashed, dotted, and dash–dotted lines are obtained with the full, contact, 1π, and 2π contributions, respectively. (e)–(g) Thick lines correspond to the results of $c_0 = 1.37$, while thin-solid, thin-dashed, and thin-dotted lines are those of $c_0 = 1.00$, 1.10, and 1.20, respectively. See text for details.

Table A1. The calculated ground-state energy of ^{4}He with $\Lambda = 450$ MeV when c_0 varies from unity to 1.37 fixed from the relative energy of the ^{8}Be-ground state.

c_0		Full	Contacts	1π	2π
1.00	E_α (MeV)	−10.7886	−3.1672	84.5460	6.5319
1.10		−16.8024	−8.4189	88.0657	2.2501
1.20		−22.8162	−13.6706	91.5853	−2.0317
1.37		−33.0397	−22.5984	97.5687	−9.3107

terms, 1π-exchange term, and 2π-exchange terms. The thick lines are the results of $c_0 = 1.37$, while those of $c_0 = 1.00$, 1.10, and 1.20 are the thin-solid, thin-dashed, and thin-dotted lines, respectively. These lines are fragmented into figures A1(a)–(d); the thin-solid, thin-dashed, thin-dotted, and thick lines in figure A1(e) are equivalent to the solid lines in figuress A1(a)–(d), respectively, and similar for the other lines in figuress A1(f)–(h). One sees that the energies associated with each contribution vary gradually with respect to the evolution of c_0.

We confirmed numerically that the similar results are obtained for $\Lambda = 500$ and 600 MeV, even though the range of the c_0 variation is rather large compared to the 450 MeV-cutoff case. Thus we confirm that our conclusion is robust against the variation of c_0.

A.2. Gaussian-range parameter

To investigate the ν dependence of $E(0^+)$, we perform the calculations with $\nu = 0.24, 0.26$, and 0.28 fm^{-2}. When ν is changed, c_0 also needs to be modified slightly to describe the measured value of the relative energy of ^{8}Be. For $\Lambda = 450$ MeV, we obtain $E(0^+)$ computed by the GCM as 0.0453, 0.135, 0.122 MeV with $(\nu, c_0) = (0.24\ \text{fm}^{-2}, 1.36)$, $(0.26\ \text{fm}^{-2}, 1.37)$, and $(0.28\ \text{fm}^{-2}, 1.39)$, respectively.

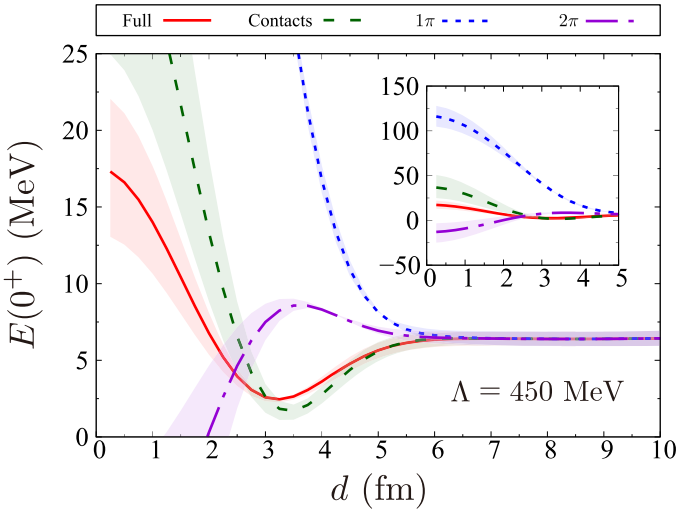

Figure A2. The ν dependence of $E(0^+)$ of ^{8}Be for the $\Lambda = 450$ MeV case. The solid, dashed, dotted, and dash–dotted lines are respectively the results for the full, contact, 1π, and 2π contributions with $\nu = 0.26$ fm^{-2}. The filled areas associated with each line are obtained when ν varies from 0.24 to 0.28 fm^{-2}. See text for details.

Table A2. The ground-state energy of ^{4}He calculated with $\Lambda = 450$ MeV for different values of ν.

ν(fm^{-2})		Full	Contacts	1π	2π
0.24	E_α (MeV)	−31.0406	−24.9839	87.2218	−2.1090
0.26		−33.0397	−22.5984	97.5687	−9.3107
0.28		−35.2337	−19.2930	108.6771	−18.3912

Figure A2 shows $E(0^+)$ of ^{8}Be as a function of d computed with $\Lambda = 450$ MeV. The legends are same as those of figure 5 but now the lines have the bands. The lines correspond to the result with $\nu = 0.26$ fm^{-2}, as those in figure 5(a). The calculations with $\nu = 0.24$ fm^{-2} ($\nu = 0.28$ fm^{-2}) determine the lower (upper) limits of the band of the full, contact, and 1π cases for small d, while they oppositely results in the upper (lower) limits for the 2π case. A breakdown of E_α computed with different ν is listed in table A2.

One finds from figure A2 that our conclusion drawn in section 3.2 remains unchanged even when ν varies; the 2π-exchange contribution is a dominant source of the attraction, the 1π-exchange one gives strong repulsion, and the contacts bring about the nonnegligible attraction at the intermediate α–α distances with mainly repulsive nature. Similar numerical calculations confirmed that the variation of ν does not affect our conclusion even for the other Λ.

Appendix B. Formulation of two-body matrix elements

B.1. General expression of matrix elements

We derive the two-body MEs of equation (10) with the antisymmetrized two-body states defined by

$$|ijab\rangle_A = \frac{1}{\sqrt{2}}\left[|\phi_i\chi_a\rangle|\phi_j\chi_b\rangle - |\phi_j\chi_b\rangle|\phi_i\chi_a\rangle\right]. \tag{B.1}$$

Owing to the spin and isospin saturation in the Brink model, only the central-force contributions of $\hat{V}_{ij}^{(\mathrm{N})}$ remain, and thus all the antisymmetrized two-body MEs are reduced to the form,

$$\begin{aligned}\sum_{a=1}^{4}\sum_{b=1}^{4}\left\langle klab\left|\hat{V}_X^{(n_\chi)}\right|ijab\right\rangle_A &= A_{ijkl}\sum_{\ell}(-)^{\ell}P_\ell(x_{ijkl}) \\ &\times \iint \mathrm{d}p\,\mathrm{d}p'\,p^2p'^2g(p,p')u_n(p,p')\,j_\ell(r_{ij}p)\,j_\ell(r_{kl}p')\,\mathcal{M}_{X;\ell}^{(n_\chi)}(p,p').\end{aligned} \tag{B.2}$$

Here the symbol X is a representative for each pion-exchange contribution ($X =$ ct, 1π, or 2π), and $\mathcal{M}_{X;\ell}^{(n_\chi)}$ is the multipole-expansion (MPE) function, the explicit form of which is given in appendix B.2. The center-of-mass contribution is factored out as A_{ijkl} defined by

$$A_{ijkl} = \frac{1}{(\pi\nu)^{\frac{3}{2}}}\exp\left[-\nu\left(\boldsymbol{R}_{ij}-\boldsymbol{R}_{kl}\right)^2\right], \tag{B.3}$$

$$\boldsymbol{R}_{ij} = \frac{1}{2}\left(\boldsymbol{R}_i+\boldsymbol{R}_j\right). \tag{B.4}$$

Two nucleons interact with each other characterized by the relative momentum $\boldsymbol{p}$ ($\boldsymbol{p}'$) in the initial channel (final channel), associated with the orbital-angular momentum ℓ. We define the relative vector,

$$\boldsymbol{r}_{ij} = \boldsymbol{R}_i - \boldsymbol{R}_j, \tag{B.5}$$

and its magnitude r_{ij}, which appears in the argument of the spherical Bessel function j_ℓ, is equivalent to the cluster distance d introduced in section 2.1. The Legendre polynomial P_ℓ has the argument x_{ijkl} defined by

$$x_{ijkl} = \begin{cases} 1 & (i=j \text{ and/or } k=l), \\ \cos\,\theta_{ijkl} = \dfrac{\boldsymbol{r}_{ij}\cdot\boldsymbol{r}_{kl}}{r_{ij}r_{kl}} & (i\neq j \text{ and } k\neq l), \end{cases} \tag{B.6}$$

with the angle θ_{ijkl} between the vectors $\boldsymbol{r}_{ij}$ and $\boldsymbol{r}_{kl}$. The function g is given by

$$g(p,p') = \exp\left[-\frac{1}{2\nu}\left(p^2+p'^2\right)\right], \tag{B.7}$$

while the regulator u_n has the nonlocal form [38] as

$$u_n(p,p') = \exp\left[-\left(\frac{p}{\Lambda}\right)^{2n}-\left(\frac{p'}{\Lambda}\right)^{2n}\right], \tag{B.8}$$

with the cutoff momentum Λ.

Equation (B.2) is the expression relevant to the calculations before the angular-momentum projection. To perform the angular-momentum projection by equation (7), we need to rotate

the two-body states $|ijab\rangle_A$. As a result, we just have to transform the vectors $\boldsymbol{R}_{ij}$ and $\boldsymbol{r}_{ij}$ as

$$\boldsymbol{R}_{ij} \to \boldsymbol{R}_{ij}^{(R)} = \frac{1}{2}\left[\hat{R}(\Omega)\boldsymbol{R}_i + \hat{R}(\Omega)\boldsymbol{R}_j\right], \tag{B.9}$$

$$\boldsymbol{r}_{ij} \to \boldsymbol{r}_{ij}^{(R)} = \hat{R}(\Omega)\boldsymbol{R}_i - \hat{R}(\Omega)\boldsymbol{R}_j. \tag{B.10}$$

The spin states are invariant under the spin-space rotation within the Brink model presuming the spin-singlet-nucleon pairs. Furthermore, we do not need to rotate the vectors $\boldsymbol{R}_{kl}$ and $\boldsymbol{r}_{kl}$ associated with the bra states, since the Hamiltonian we employ is rotationally invariant.

Note that it is necessary to multiply the conventional chiral potential [38] by $1/(2\pi)^3$, originating from our convention of the normalization, $\langle \boldsymbol{p}|\boldsymbol{p}'\rangle = \delta(\boldsymbol{p}-\boldsymbol{p}')$. See references [78, 79] for similar prefactors involved in the chiral three-nucleon potential.

B.2. Multipole-expansion function

The potential of the chiral interaction defined in the momentum space depends on $\boldsymbol{p}$ and $\boldsymbol{p}'$ [38], or equivalently the magnitude of the transferred momentum $\boldsymbol{q}$ and the average momentum $\boldsymbol{Q}$, respectively defined by

$$\boldsymbol{q} = \boldsymbol{p}' - \boldsymbol{p}, \tag{B.11}$$

$$\boldsymbol{Q} = \frac{1}{2}\left(\boldsymbol{p} + \boldsymbol{p}'\right). \tag{B.12}$$

We perform the MPE with respect to $x = \cos\theta$ with the angle θ between $\boldsymbol{p}$ and $\boldsymbol{p}'$. Note that we do not need to perform the MPE for the contact terms, while for the long-range terms, we need to do so. More explicitly, for the former, the angular integration in the MPE function can be done analytically owing to the absence of the pion propagator. However, for the latter, the pion propagator prevents from performing the integration analytically, and therefore numerical integration is necessary.

The LECs involved in the MPE functions defined below are explicitly given in appendix C. Let us start to write the MPE function of the contact terms at LO as

$$\mathcal{M}^{(0)}_{\mathrm{ct};\ell}(p,p') = \frac{4}{\pi}\left[C_{\mathrm{S}}^{\mathrm{pp}} + C_{\mathrm{S}}^{\mathrm{nn}} + 4C_{\mathrm{S}}^{\mathrm{nn}} - 3\left(C_{\mathrm{T}}^{\mathrm{pp}} + C_{\mathrm{T}}^{\mathrm{nn}}\right)\right]\delta_{\ell 0}, \tag{B.13}$$

where the LECs C_{S} and C_{T} depend on the nucleon charge. Obviously there is only the s-wave contribution here, and it is natural since ℓ contributing to the pure contact terms at LO should be zero.

The next term is the 1π-exchange contribution at LO, the MPE function of which reads,

$$\mathcal{M}^{(0)}_{1\pi;\ell}(p,p') = \frac{6}{\pi}\left(\frac{g_{\mathrm{A}}}{f_\pi}\right)^2\frac{\hat{\ell}^2}{2}\int_{-1}^{1}\mathrm{d}x\,P_\ell(x)\frac{q^2}{q^2+m_\pi^2}, \tag{B.14}$$

where g_{A}, f_π, and m_π are the axial vector coupling constant, the pion-decay constant, and the average pion mass, respectively. Their values, the average nucleon mass m_{N} as well, are summarized in appendix C. We adopt the abbreviation $\hat{\ell} = \sqrt{2\ell+1}$.

At NLO of the contact terms, the p wave starts to contribute as

$$\begin{aligned}\mathcal{M}^{(2)}_{\mathrm{ct};\ell}(p,p') = \frac{2}{\pi}\big[&(12C_1 + 3C_2 - 12C_3 - 3C_4 - 4C_6 - C_7)(p^2+p'^2)\delta_{\ell 0}\\ &+ 2\,(20C_1 - 5C_2 + 12C_3 - 3C_4 + 4C_6 - C_7)\,pp'\delta_{\ell 1}\big],\end{aligned} \tag{B.15}$$

where C_i are the LECs.

The MPE function of the 2π-exchange terms at NLO is expressed by

$$\mathcal{M}^{(2)}_{2\pi;\ell}(p,p') = \frac{1}{(2\pi)^3 f_\pi^4}\frac{\hat{\ell}^2}{2}\int_{-1}^{1} \mathrm{d}x\, P_\ell(x)\left[W^{(2)}_{\mathrm{C}}(q,Q) + V^{(2)}_{\mathrm{S}}(q,Q)\right], \tag{B.16}$$

$$W^{(2)}_{\mathrm{C}}(q,Q) = \frac{1}{2}L(q)\left[4m_\pi^2\left(5g_{\mathrm{A}}^4 - 4g_{\mathrm{A}}^2 - 1\right) + q^2\left(23g_{\mathrm{A}}^4 - 10g_{\mathrm{A}}^2 - 1\right) + 48g_{\mathrm{A}}^4 m_\pi^4 w^{-2}\right], \tag{B.17}$$

$$V^{(2)}_{\mathrm{S}}(q,Q) = -6g_{\mathrm{A}}^4 q^2 L(q), \tag{B.18}$$

and

$$L(q) = \frac{w}{q}\ln\frac{w+q}{2m_\pi}, \tag{B.19}$$

$$w = \sqrt{4m_\pi^2 + q^2}. \tag{B.20}$$

At N^{2}LO we have

$$\mathcal{M}^{(3)}_{2\pi;\ell}(p,p') = \frac{3g_{\mathrm{A}}^2}{(4\pi)^2 f_\pi^4}\frac{\hat{\ell}^2}{2}\int_{-1}^{1} \mathrm{d}x\, P_\ell(x)\left[\left\{4(-)^\ell - 1\right\} V^{(3)}_{\mathrm{C}}(q,Q) + W^{(3)}_{\mathrm{C}}(q,Q) + V^{(3)}_{\mathrm{S}}(q,Q) + W^{(3)}_{\mathrm{S}}(q,Q)\right], \tag{B.21}$$

$$V^{(3)}_{\mathrm{C}}(q,Q) = 8\left[\frac{g_{\mathrm{A}}^2 m_\pi^5}{16m_{\mathrm{N}}w^2} - \left\{2m_\pi^2(2c_1 - c_3) - q^2\left(c_3 + \frac{3g_{\mathrm{A}}^2}{16m_{\mathrm{N}}}\right)\right\}\tilde{w}^2 A \times (q) - \frac{g_{\mathrm{A}}^2}{16m_{\mathrm{N}}}\left\{m_\pi w^2 + \tilde{w}^4 A(q)\right\}\right], \tag{B.22}$$

$$W^{(3)}_{\mathrm{C}}(q,Q) = -\frac{1}{m_{\mathrm{N}}}\left[3g_{\mathrm{A}}^2 m_\pi^5 w^{-2} - \left\{4m_\pi^2 + 2q^2 - g_{\mathrm{A}}^2\left(4m_\pi^2 + 3q^2\right)\right\}\tilde{w}^2 A(q) + g_{\mathrm{A}}^2\left\{m_\pi w^2 + \tilde{w}^4 A(q)\right\}\right], \tag{B.23}$$

$$V^{(3)}_{\mathrm{S}}(q,Q) = \frac{g_{\mathrm{A}}^2}{2m_{\mathrm{N}}}\left[3q^2\tilde{w}^2 A(q) + q^2\left\{m_\pi + w^2 A(q)\right\}\right], \tag{B.24}$$

$$W^{(3)}_{\mathrm{S}}(q,Q) = -8\left[q^2 A(q)\left\{\left(c_4 + \frac{1}{4m_{\mathrm{N}}}\right)w^2 - \frac{g_{\mathrm{A}}^2}{8m_{\mathrm{N}}}\left(10m_\pi^2 + 3q^2\right)\right\} + \frac{g_{\mathrm{A}}^2}{8m_{\mathrm{N}}}q^2\left\{m_\pi + w^2 A(q)\right\}\right], \tag{B.25}$$

with the LECs c_i, and

$$A(q) = \frac{1}{2q}\arctan\frac{q}{2m_\pi}, \tag{B.26}$$

$$\tilde{w} = \sqrt{2m_\pi^2 + q^2}. \tag{B.27}$$

The contact terms at N^{3}LO is characterized by

$$
\begin{aligned}
\mathcal{M}^{(4)}_{\mathrm{ct};\ell}(p,p') = \frac{1}{\pi}\Bigg[&\left(24D_1+\frac{3}{2}D_2-24D_5-\frac{3}{2}D_6-8D_{11}-\frac{1}{2}D_{14}\right)\\
&\times\left\{(p^2+p'^2)^2+\frac{4}{3}p^2p'^2\right\}\delta_{\ell 0}\\
&+(6D_3+4D_4-6D_7-4D_8-2D_{12}-2D_{13})\times\left\{(p^2+p'^2)^2-\frac{4}{3}p^2p'^2\right\}\delta_{\ell 0}\\
&+4\left(40D_1-\frac{5}{2}D_2+24D_5-\frac{3}{2}D_6+8D_{11}+\frac{1}{2}D_{14}\right)pp'(p^2+p'^2)\delta_{\ell 1}\\
&+\frac{8}{3}\Bigg(24D_1+\frac{3}{2}D_2-6D_3-4D_4-24D_5-\frac{3}{2}D_6+6D_7+4D_8-8D_{11}\\
&+2D_{12}+2D_{13}-\frac{1}{2}D_{14}\Bigg)p^2p'^2\delta_{\ell 2}\Bigg]-\frac{1}{15\pi}\left[\left\{16(-)^\ell-4\right\}D_4-12D_8\right]\\
&\times\sum_{\Lambda_q=0}^{2}\sum_{\Lambda_Q=0}^{2}(-)^{\Lambda_Q}\widehat{2-\Lambda_q}\widehat{2-\Lambda_Q}\left[\binom{5}{2\Lambda_q}\binom{5}{2\Lambda_Q}\right]^{\frac{1}{2}}\left(\Lambda_q 0\Lambda_Q 0|\ell 0\right)\\
&\times\left(2-\Lambda_q,0,2-\Lambda_Q,0|\ell 0\right)\begin{Bmatrix}\Lambda_q & 2-\Lambda_q & 2\\ 2-\Lambda_Q & \Lambda_Q & \ell\end{Bmatrix}p^{\Lambda_q+\Lambda_Q}p'^{4-\Lambda_q-\Lambda_Q}\\
&+\frac{288}{\pi}D_{15}\sum_{L_q=0,2}\left(-\frac{1}{2}\right)^{L_q}\left(1010|L_q0\right)^2\begin{Bmatrix}1 & 1 & 1\\ 1 & 1 & L_q\end{Bmatrix}\\
&\times\sum_{\lambda_q=0}^{\Lambda_q}\sum_{\lambda_Q=0}^{\Lambda_Q}(-)^{\lambda_Q}\widehat{L_q-\lambda_q}\widehat{L_q-\lambda_Q}\left[\binom{2L_q+1}{2\lambda_q}\binom{2L_q+1}{2\lambda_Q}\right]^{\frac{1}{2}}\\
&\times\sum_{\lambda K}\left(\lambda_q 0\lambda_Q 0|\lambda 0\right)\left(L_q-\lambda_q,0,L_q-\lambda_Q,0|\lambda 0\right)\left(\lambda 0\ K0|\ell 0\right)^2\\
&\times\begin{Bmatrix}\lambda_q & L_q-\lambda_q & L_q\\ L_q-\lambda_Q & \lambda_Q & \lambda\end{Bmatrix}p^{\lambda_q+\lambda_Q}p'^{\,2L_q-\lambda_q-\lambda_Q}\\
&\times\left[\frac{1}{4}\left[\left\{\left(p^2+p'^2\right)^2-\frac{4}{3}p^2p'^2\right\}\delta_{K0}-\frac{8}{3}p^2p'^2\delta_{K2}\right]\delta_{L_q0}+\delta_{K0}\delta_{L_q2}\right],
\end{aligned}
\tag{B.28}
$$

where D_i are the LECs and the binomial coefficient is defined by

$$
\binom{n_1}{n_2}=\frac{n_1!}{(n_1-n_2)!n_2!}. \tag{B.29}
$$

As regards the 2π-exchange terms at N^{3}LO, it is convenient to classify the MPE function into the c_i^2, c_i/m_{N}, m_{N}^{-2}, and two-loop (2L) terms [38];

$$
\begin{aligned}
\mathcal{M}^{(4)}_{2\pi;\ell}(p,p') = &\mathcal{M}^{(c_i^2)}_{2\pi;\ell}(p,p')+\mathcal{M}^{(c_i/m_{\mathrm{N}})}_{2\pi;\ell}(p,p')\\
&+\mathcal{M}^{(m_{\mathrm{N}}^{-2})}_{2\pi;\ell}(p,p')+\mathcal{M}^{(\mathrm{2L})}_{2\pi;\ell}(p,p').
\end{aligned}
\tag{B.30}
$$

Then, the MPE of the c_i^2 terms reads

$$\mathcal{M}_{2\pi;\ell}^{(c_i^2)}(p,p') = \frac{1}{2\pi^3 f_\pi^4}\frac{\hat{\ell}^2}{2}\int_{-1}^{1}\mathrm{d}x\,P_\ell(x)\left[\left\{4(-)^\ell-1\right\}V_{\mathrm{C}}^{(c_i^2)}(q,Q)+W_{\mathrm{S}}^{(c_i^2)}(q,Q)\right], \quad \text{(B.31)}$$

$$V_{\mathrm{C}}^{(c_i^2)}(q,Q) = 3L(q)\left[\left(\frac{c_2}{6}w^2+c_3\tilde{w}^2-4c_1m_\pi^2\right)^2+\frac{c_2^2}{45}w^4\right], \quad \text{(B.32)}$$

$$W_{\mathrm{S}}^{(c_i^2)}(q,Q) = c_4^2q^2w^2L(q), \quad \text{(B.33)}$$

while that of the c_i/m_{N} terms is given by

$$\mathcal{M}_{2\pi;\ell}^{(c_i/m_{\mathrm{N}})}(p,p') = -\frac{1}{(2\pi)^3 m_{\mathrm{N}} f_\pi^4}\frac{\hat{\ell}^2}{2}\int_{-1}^{1}\mathrm{d}x\,P_\ell(x) \times\left[\left\{4(-)^\ell-1\right\}V_{\mathrm{C}}^{(c_i/m_{\mathrm{N}})}(q,Q)+W_{\mathrm{C}}^{(c_i/m_{\mathrm{N}})}(q,Q)+W_{\mathrm{S}}^{(c_i/m_{\mathrm{N}})}(q,Q),\right. \quad \text{(B.34)}$$

$$V_{\mathrm{C}}^{(c_i/m_{\mathrm{N}})}(q,Q) = 2g_{\mathrm{A}}^2L(q)\left[(c_2-6c_3)q^4+4(6c_1+c_2-3c_3)q^2m_\pi^2 +6(c_2-2c_3)m_\pi^4+24(2c_1+c_3)m_\pi^6w^{-2}\right], \quad \text{(B.35)}$$

$$W_C^{(c_i/m_{\mathrm{N}})}(q,Q) = -c_4q^2L(q)\left[g_{\mathrm{A}}^2\left(8m_\pi^2+5q^2\right)+w^2\right], \quad \text{(B.36)}$$

$$W_{\mathrm{S}}^{(c_i/m_{\mathrm{N}})}(q,Q) = 2c_4q^2L(q)\left[g_{\mathrm{A}}^2\left(16m_\pi^2+7q^2\right)-w^2\right]. \quad \text{(B.37)}$$

The m_{N}^{-2} terms have the MPE function of the form,

$$\mathcal{M}_{2\pi;\ell}^{(m_{\mathrm{N}}^{-2})}(p,p') = -\frac{1}{(2\pi)^3 m_{\mathrm{N}}^2 f_\pi^4}\frac{\hat{\ell}^2}{2}\int_{-1}^{1}\mathrm{d}x\,P_\ell(x) \times\left[\left\{4(-)^\ell-1\right\}V_{\mathrm{C}}^{(m_{\mathrm{N}}^{-2})}(q,Q)+W_{\mathrm{C}}^{(m_{\mathrm{N}}^{-2})}(q,Q)\right. +\left.V_{\mathrm{S}}^{(m_{\mathrm{N}}^{-2})}(q,Q)+W_{\mathrm{S}}^{(m_{\mathrm{N}}^{-2})}(q,Q)\right]+\mathcal{M}_{\sigma L;\ell}^{(m_{\mathrm{N}}^{-2})}(p,p'), \quad \text{(B.38)}$$

$$V_{\mathrm{C}}^{(m_{\mathrm{N}}^{-2})}(q,Q) = 2g_{\mathrm{A}}^4L(q)\left[\left(2m_\pi^8w^{-4}+8m_\pi^6w^{-2}-q^4-2m_\pi^4\right)+\frac{1}{2}m_\pi^6w^{-2}\right], \quad \text{(B.39)}$$

$$W_{\mathrm{C}}^{(m_{\mathrm{N}}^{-2})}(q,Q) = -\frac{1}{4}L(q)\left[8g_{\mathrm{A}}^2\left\{\frac{3}{2}q^4+3m_\pi^2q^2+3m_\pi^4-6m_\pi^6w^{-2} -Q^2\left(8m_\pi^2+5q^2\right)\right\}+4g_{\mathrm{A}}^4\left\{Q^2\left(20m_\pi^2+7q^2-16m_\pi^4w^{-2}\right)\right. +16m_\pi^8w^{-4}+12m_\pi^6w^{-2}-4m_\pi^4q^2w^{-2}-5q^4 -\left.6m_\pi^2q^2-6m_\pi^4\right\}-4Q^2w^2\Big]-4g_{\mathrm{A}}^4m_\pi^6w^{-2}, \quad \text{(B.40)}$$

$$V_{\mathrm{S}}^{(m_{\mathrm{N}}^{-2})}(q,Q) = -4g_{\mathrm{A}}^4q^2L(q)\left[Q^2+\frac{5}{8}q^2+m_\pi^4w^{-2}\right], \quad \text{(B.41)}$$

$$W_{\rm S}^{(m_{\rm N}^{-2})}(q,Q) = -\frac{1}{4}q^2L(q)\left[4g_{\rm A}^4\left(7m_\pi^2+\frac{17}{4}q^2+4m_\pi^4w^{-2}\right)\right.$$
$$\left.-32g_{\rm A}^2\left(m_\pi^2+\frac{7}{16}q^2\right)+w^2\right], \tag{B.42}$$

$$\mathcal{M}_{\sigma L;\ell}^{(m_{\rm N}^{-2})}(p,p') = \frac{9g_{\rm A}^4}{\pi^3m_{\rm N}^2f_\pi^4}\sum_{L_q=0,2}\left(-\frac{1}{2}\right)^{L_q}(1010|L_q0)^2\begin{Bmatrix}1&1&1\\1&1&L_q\end{Bmatrix}$$
$$\times\sum_{\lambda_q=0}^{\Lambda_q}\sum_{\lambda_Q=0}^{\Lambda_Q}(-)^{\lambda_Q}\widehat{L_q-\lambda_q}\widehat{L_q-\lambda_Q}\left[\begin{pmatrix}2L_q+1\\2\lambda_q\end{pmatrix}\begin{pmatrix}2L_q+1\\2\lambda_Q\end{pmatrix}\right]^{\frac{1}{2}}$$
$$\times\sum_{\lambda K}(\lambda_q0\lambda_Q0|\lambda0)\left(L_q-\lambda_q,0,L_q-\lambda_Q,0|\lambda0\right)\left(\lambda0K0|\ell0\right)^2$$
$$\times\begin{Bmatrix}\lambda_q&L_q-\lambda_q&L_q\\L_q-\lambda_Q&\lambda_Q&\lambda\end{Bmatrix}p^{\lambda_q+\lambda_Q}p'^{\,2L_q-\lambda_q-\lambda_Q}$$
$$\times\frac{\hat{K}^2}{2}\int_{-1}^{1}{\rm d}x\,P_K(x)q^{2-L_q}Q^{2-L_q}L(q). \tag{B.43}$$

Lastly, we write the MPE function of the 2L terms as

$$\mathcal{M}_{2\pi;\ell}^{(2{\rm L})}(p,p') = \frac{1}{16(2\pi)^3f_\pi^6}\frac{\hat{\ell}^2}{2}\int_{-1}^{1}{\rm d}x\,P_\ell(x)\left[\left\{4(-)^\ell-1\right\}V_{\rm C}^{(2{\rm L})}(q,Q)\right.$$
$$\left.+W_{\rm C}^{(2{\rm L})}(q,Q)+V_{\rm S}^{(2{\rm L})}(q,Q)+W_{\rm S}^{(2{\rm L})}(q,Q)\right], \tag{B.44}$$

$$V_{\rm C}^{(2{\rm L})}(q,Q) = 3g_{\rm A}^4\tilde{w}^2A(q)\left[\left(m_\pi^2+2q^2\right)\left(2m_\pi+\tilde{w}^2A(q)\right)+4g_{\rm A}^2m_\pi\tilde{w}^2\right], \tag{B.45}$$

$$W_{\rm C}^{(2{\rm L})}(q,Q) = -\frac{1}{6\pi^2}L(q)\left[192\pi^2f_\pi^2w^2\bar{d}_3\left\{2g_{\rm A}^2\tilde{w}^2-\frac{3}{5}\left(g_{\rm A}^2-1\right)w^2\right\}\right.$$
$$+\left\{6g_{\rm A}^2\tilde{w}^2-\left(g_{\rm A}^2-1\right)w^2\right\}$$
$$\times\left[384\pi^2f_\pi^2\left\{\tilde{w}^2\left(\bar{d}_1+\bar{d}_2\right)+4m_\pi^2\bar{d}_5\right\}+L(q)\left\{4m_\pi^2\left(1+2g_{\rm A}^2\right)\right.\right.$$
$$\left.\left.\left.+q^2\left(1+5g_{\rm A}^2\right)\right\}-\frac{1}{3}q^2\left(5+13g_{\rm A}^2\right)-8m_\pi^2\left(1+2g_{\rm A}^2\right)\right]\right], \tag{B.46}$$

$$V_{\rm S}^{(2{\rm L})}(q,Q) = -64g_{\rm A}^2f_\pi^2\left(\bar{d}_{14}-\bar{d}_{15}\right)q^2w^2L(q), \tag{B.47}$$

$$W_{\rm S}^{(2{\rm L})}(q,Q) = 3g_{\rm A}^4q^2w^2A(q)\left[w^2A(q)+2m_\pi\left(1+2g_{\rm A}^2\right)\right], \tag{B.48}$$

where $\bar{d}_i$ are the LECs.

Appendix C. Constants

The constants necessary for the ME calculations are the average nucleon mass $m_{\rm N}$, the average pion mass m_π, the pion-decay constant f_π, the axial vector coupling constant $g_{\rm A}$, and LECs $\left(C_{\rm S},C_{\rm T},C_i,D_i,c_i,\text{and }\bar{d}_i\right)$, as well as the regulator parameters (the exponent n and the

Table C1. The average masses ($m_{\rm N}$ and m_π) and the pion-decay constant f_π are in units of MeV, while the axial vector coupling constant $g_{\rm A}$ is dimensionless.

$m_{\rm N}$	m_π	f_π	$g_{\rm A}$
938.9187	138.0394	92.4	1.29

Table C2. The regulator parameter n and the LECs for three sets of Λ. The LECs c_i and $\bar{d}_i$ involved in the 2π-exchange terms are respectively in units of GeV^{-1} and GeV^{-2}, while $C_{\rm S}$ and $C_{\rm T}$ at LO having the charge dependence are in units of 10^4 GeV^{-2}. The LECs C_i at NLO and D_i at N^{3}LO are in units of 10^4 GeV^{-4} and 10^4 GeV^{-6}, respectively.

		$\Lambda = 450$ MeV	$\Lambda = 500$ MeV	$\Lambda = 600$ MeV
	1π term	4	4	4
	LO contacts	3	3	3
n	All other terms	3	2	2
c_1		−0.81	−0.81	−0.81
c_2		3.28	2.80	2.80
c_3		−3.40	−3.20	−3.20
c_4		3.40	5.40	5.40
$\bar{d}_1 + \bar{d}_2$		3.06	3.06	3.06
$\bar{d}_3$		−3.27	−3.27	−3.27
$\bar{d}_5$		0.45	0.45	0.45
$\bar{d}_{14} - \bar{d}_{15}$		−5.65	−5.65	−5.65
$C_{\rm S}^{\rm pp}$		−0.011 603	−0.009 991	−0.009 943
$C_{\rm S}^{\rm nn}$		−0.011 610	−0.010 011	−0.009 949
$C_{\rm S}^{\rm np}$		−0.011 619	−0.010 028	−0.009 955
$C_{\rm T}^{\rm pp}$		0.000 229	0.000 523	0.000 695
$C_{\rm T}^{\rm nn}$		0.000 236	0.000 543	0.000 701
$C_{\rm T}^{\rm np}$		0.000 245	0.000 561	0.000 707
C_1		0.055 936	0.051 949	0.046 433
C_2		0.092 976	0.163 34	0.174 354
C_3		−0.003 346	0.003 249	0.006 562
C_4		−0.045 017	−0.048 954	−0.050 066
C_5		−0.072 187	−0.075 081	−0.086 978
C_6		−0.004 651	−0.013 343	−0.013 639
C_7		−0.173 839	−0.225 500	−0.214 188
D_1		0.027 479	−0.016 761	−0.026 710
D_2		2.573 138	2.478 838	3.054 553
D_3		1.773 384	0.915 937	0.100 079
D_4		−1.735 485	−0.810 894	−0.047 571
D_5		0.132 598	0.144 506	0.131 379
D_6		1.810 399	1.324 597	1.324 064
D_7		0.608 374	0.103 610	0.236 467
D_8		−0.512 382	−0.189 115	−0.268 515
D_9		−0.462 892	−0.547 244	−0.633 636
D_{10}		1.717 083	2.502 115	2.152 571
D_{11}		−0.123 624	−0.129 033	−0.154 661
D_{12}		−0.069 623	0.110 915	−0.121 515
D_{13}		−0.101 480	−0.012 318	−0.010 343
D_{14}		−0.916 369	−1.368 423	−0.860 344
D_{15}		−0.051 120	0.147 177	−0.013 131

cutoff Λ). These constants are listed in tables C1 and C2. We employ natural units in which one assumes $\hbar = 1$ and $c = 1$.

The LECs of $\Lambda = 500$ and 600 MeV are taken from reference [38]. Note that the LECs D_i listed in table F.1 of reference [38] are slightly modified because $n = 2$ is now used consistently for all fourth order contact terms [80]. The new values of D_i are given in table C2. We also test the lower-cutoff parameters, $\Lambda = 450$ MeV [54, 55], which are now represented by the partial-wave-independent expression [80].

ORCID iDs

Tokuro Fukui https://orcid.org/0000-0003-3288-5571

References

[1] Bandō H, Nagata S and Yamamoto Y 1970 *Prog. Theor. Phys.* **44** 646–62
[2] Bandō H, Nagata S and Yamamoto Y 1971 *Prog. Theor. Phys.* **45** 1515–26
[3] Yamamoto Y, Bando H and Nagata S 1978 *Prog. Theor. Phys.* **59** 817–30
[4] Togashi T and Katō K 2007 *Prog. Theor. Phys.* **117** 189–94
[5] Togashi T, Murakami T and Kato K 2009 *Prog. Theor. Phys.* **121** 299–317
[6] Yamamoto Y, Togashi T and Kato K 2010 *Prog. Theor. Phys.* **124** 315–30
[7] Togashi T and Katō K 2012 *Antisymmetrized Molecular Dynamics with Bare Nuclear Interactions: Brueckner-AMD, and its Applications to Light Nuclei* (Rijeka: InTech)
[8] Wiringa R B, Pieper S C, Carlson J and Pandharipande V R 2000 *Phys. Rev.* C **62** 014001
[9] Carlson J, Gandolfi S, Pederiva F, Pieper S C, Schiavilla R, Schmidt K E and Wiringa R B 2015 *Rev. Mod. Phys.* **87** 1067–118
[10] Datar V M *et al* 2013 *Phys. Rev. Lett.* **111** 062502
[11] Navrátil P, Vary J P and Barrett B R 2000 *Phys. Rev. Lett.* **84** 5728–31
[12] Navrátil P, Vary J P and Barrett B R 2000 *Phys. Rev.* C **62** 054311
[13] Abe T, Maris P, Otsuka T, Shimizu N, Utsuno Y and Vary J P 2012 *Phys. Rev.* C **86** 054301
[14] Shimizu N, Abe T, Tsunoda Y, Utsuno Y, Yoshida T, Mizusaki T, Honma M and Otsuka T 2012 *Prog. Theor. Exp. Phys.* **2012** 01A205
[15] Hupin G, Quaglioni S and Navrátil P 2015 *Phys. Rev. Lett.* **114** 212502
[16] Kravvaris K and Volya A 2017 *Phys. Rev. Lett.* **119** 062501
[17] Dytrych T, Sviratcheva K D, Bahri C, Draayer J P and Vary J P 2007 *Phys. Rev. Lett.* **98** 162503
[18] Dytrych T *et al* 2013 *Phys. Rev. Lett.* **111** 252501
[19] Dreyfuss A C, Launey K D, Escher J E, Sargsyan G H, Baker R B, Dytrych T and Draayer J P 2020 *Phys. Rev.* C **102** 044608
[20] Romero-Redondo C, Quaglioni S, Navrátil P and Hupin G 2014 *Phys. Rev. Lett.* **113** 032503
[21] Kravvaris K, Quaglioni S, Hupin G and Navratil P 2020 *Ab initio* framework for nuclear scattering and reactions induced by light projectiles (arXiv:2012.00228)
[22] Romero-Redondo C, Quaglioni S, Navrátil P and Hupin G 2016 *Phys. Rev. Lett.* **117** 222501
[23] Neff T and Feldmeier H 2004 *Nucl. Phys.* A **738** 357–61
[24] Chernykh M, Feldmeier H, Neff T, von Neumann-Cosel P and Richter A 2007 *Phys. Rev. Lett.* **98** 032501
[25] Borasoy B, Epelbaum E, Krebs H, Lee D and Meißner U-G 2007 *Eur. Phys. J.* A **31** 105–23
[26] Borasoy B, Epelbaum E, Krebs H, Lee D and Meißner U-G 2007 *Eur. Phys. J.* A **34** 185–96
[27] Epelbaum E, Krebs H, Lee D and Meißner U-G 2011 *Phys. Rev. Lett.* **106** 192501
[28] Epelbaum E, Krebs H, Lähde T A, Lee D and Meißner U-G 2012 *Phys. Rev. Lett.* **109** 252501
[29] Epelbaum E, Krebs H, Lähde T A, Lee D and Meißner U-G 2013 *Eur. Phys. J.* A **49** 82
[30] Epelbaum E, Krebs H, Lähde T A, Lee D, Meißner U-G and Rupak G 2014 *Phys. Rev. Lett.* **112** 102501
[31] Elhatisari S, Lee D, Rupak G, Epelbaum E, Krebs H, Lähde T A, Luu T and Meißner U-G 2015 *Nature* **528** 111–4
[32] Elhatisari S *et al* 2016 *Phys. Rev. Lett.* **117** 132501

[33] Elhatisari S, Epelbaum E, Krebs H, Lähde T A, Lee D, Li N, Lu B-n, Meißner U-G and Rupak G 2017 *Phys. Rev. Lett.* **119** 222505
[34] Freer M, Horiuchi H, Kanada-En'yo Y, Lee D and Meißner U G 2018 *Rev. Mod. Phys.* **90** 035004
[35] Shimodaya I o, Tamagaki R o o and Tanaka H 1962 *Prog. Theor. Phys.* **27** 793–810
[36] Weinberg S 1979 *Physica* A **96** 327–40
[37] Epelbaum E 2006 *Prog. Part. Nucl. Phys.* **57** 654–741
[38] Machleidt R and Entem D R 2011 *Phys. Rep.* **503** 1–75
[39] Ikeda K, Marumori T, Tamagaki R and Tanaka H 1972 *Prog. Theor. Phys. Suppl.* **52** 1–24
[40] Hiura J and Tamagaki R 1972 *Prog. Theor. Phys. Suppl.* **52** 25–88
[41] Volkov A B 1965 *Nucl. Phys.* **74** 33–58
[42] Brink D M 1966 *The Alpha-Particle Model of Light Nuclei* (New York: Academic)
[43] Entem D R and Machleidt R 2002 *Phys. Lett.* B **524** 93–8
[44] Entem D R and Machleidt R 2002 *Phys. Rev.* C **66** 014002
[45] Entem D R and Machleidt R 2003 *Phys. Rev.* C **68** 041001
[46] Hill D L and Wheeler J A 1953 *Phys. Rev.* **89** 1102–45
[47] Griffin J J and Wheeler J A 1957 *Phys. Rev.* **108** 311–27
[48] Mito Y and Kamimura M 1976 *Prog. Theor. Phys.* **56** 583–98
[49] Kamimura M 1977 *Prog. Theor. Phys. Suppl.* **62** 236–94
[50] Matsuno H, Kanada-En'yo Y and Itagaki N 2018 *Phys. Rev.* C **98** *054306*
[51] Itagaki N, Matsuno H and Kanada-En'o Y 2019 *Prog. Theor. Exp. Phys.* **2019** 063D02
[52] Angeli I and Marinova K P 2013 *At. Data Nucl. Data Tables* **99** 69–95
[53] Borisyuk D 2010 *Nucl. Phys.* A **843** 59–67
[54] Coraggio L, Holt J W, Itaco N, Machleidt R and Sammarruca F 2013 *Phys. Rev.* C **87** 014322
[55] Coraggio L, Holt J W, Itaco N, Machleidt R, Marcucci L E and Sammarruca F 2014 *Phys. Rev.* C **89** 044321
[56] Wang M, Huang W J, Kondev F G, Audi G and Naimi S 2021 *Chin. Phys.* C **45** 030003
[57] Tilley D R, Kelley J H, Godwin J L, Millener D J, Purcell J E, Sheu C G and Weller H R 2004 *Nucl. Phys.* A **745** 155–362
[58] Itagaki N, Fukui T and Tohsaki A 2020 Challenge for describing the cluster states starting with realistic interaction (arXiv:2003.08546)
[59] Tohsaki A 1994 *Phys. Rev.* C **49** 1814–7
[60] Heydenburg N P and Temmer G M 1956 *Phys. Rev.* **104** 123–34
[61] Russell J L, Phillips G C and Reich C W 1956 *Phys. Rev.* **104** 135–42
[62] Nilson R, Jentschke W K, Briggs G R, Kerman R O and Snyder J N 1958 *Phys. Rev.* **109** 850–60
[63] Jones C M, Phillips G C and Miller P D 1960 *Phys. Rev.* **117** 525–30
[64] Miyake K 1961 *Bull. Inst. Chem. Res. Kyoto Univ.* **39** 313
[65] Tombrello T A and Senhouse L S 1963 *Phys. Rev.* **129** 2252–8
[66] Bacher A D, Resmini F G, Conzett H E, de Swiniarski R, Meiner H and Ernst J 1972 *Phys. Rev. Lett.* **29** 1331–3
[67] Tanabe F, Tohsaki A and Tamagaki R 1975 *Prog. Theor. Phys.* **53** 677–91
[68] Hasegawa A and Nagata S 1971 *Prog. Theor. Phys.* **45** 1786–807
[69] Tamagaki R 1968 *Prog. Theor. Phys. Suppl.* **E68** 242–58
[70] Saito S 1977 *Prog. Theor. Phys. Suppl.* **62** 11–89
[71] Horiuchi H 1977 *Prog. Theor. Phys. Suppl.* **62** 90–190
[72] Fukui T, Taniguchi Y, Suhara T, Kanada-En'yo Y and Ogata K 2016 *Phys. Rev.* C **93** 034606
[73] Machleidt R 1989 *The Meson Theory of Nuclear Forces and Nuclear Structure* (Berlin: Springer) pp 189–376
[74] Machleidt R 2001 *Phys. Rev.* C **63** 024001
[75] van Kolck U 1994 *Phys. Rev.* C **49** 2932–41
[76] Epelbaum E, Nogga A, Glöckle W, Kamada H, Meißner U G and Witała H 2002 *Phys. Rev.* C **66** 064001
[77] Maris P, Vary J P and Navrátil P 2013 *Phys. Rev.* C **87** 014327
[78] Navrátil P 2007 *Few-Body Syst.* **41** 117–40
[79] Fukui T, De Angelis L, Ma Y Z, Coraggio L, Gargano A, Itaco N and Xu F R 2018 *Phys. Rev.* C **98** 044305
[80] Machleidt R 2020 private communication